ELSEVIER

Journal of Power Sources 79 (1999) 231–237

JOURNAL OF POWER SOURCES

Synthesis and characterization of spinel $LiMn_{2-x}Ni_xO_4$ for lithium/polymer battery applications

Yang-Kook Sun *, Dong-Won Kim, Young-Min Choi

Polymer Materials Laboratory, Chemical Sector, Samsung Advanced Institute of Technology, 103-12 Moonji-Dong, Yusong-Gu, Daejon 305-380, South Korea

Received 27 November 1998; accepted 27 January 1999

Abstract

Spinel $LiMn_2O_4$ and $LiMn_{1.95}Ni_{0.05}O_4$ powders with sub-micron, narrow-size-distribution, and phase-pure particles are synthesized by a sol–gel method. The effects of heat treatment on the physicochemical properties of the spinel $LiMn_2O_4$ powder are examined with X-ray diffractometry, the Brunauer–Emmett–Teller method and scanning electron microscopy. For lithium/polymer battery applications, the $LiMn_2O_4$ and $LiMn_{1.95}Ni_{0.05}O_4$ electrodes are characterized electrochemically by charge–discharge experiments and a.c.-impedance spectroscopy. Although the Ni-doped electrode has a smaller initial capacity of 126 mA h g^{-1}, it exhibits better cycling performance than the conventional electrode which delivers a higher initial capacity of 145 mA h g^{-1}. The improvement in cycling performance of the former electrode is attributed to stabilization of the spinel structure by the presence of nickel ion. The cycling performance of a Li/polymer electrolyte/$LiMn_{1.95}Ni_{0.05}O_4$ cell at various temperatures is discussed in terms of interfacial resistance and lithium-ion diffusion determined by a.c.-impedance spectroscopy.

Keywords: Lithium/polymer battery; Lithium manganese oxide; Sol–gel method; Chelating agent; Glycolic acid; Chemical diffusion of Li ion

1. Introduction

Spinel $LiMn_2O_4$ has been studied extensively as a promising cathode (positive electrode) material for lithium secondary batteries with high specific energy. This material offers several distinct advantages: it is easier to prepare, and is less expensive and less toxic than layered oxides such as $LiCoO_2$ and $LiNiO_2$ [1,2]. The electrochemical properties of $LiMn_2O_4$ powders depend strongly on the method of synthesis. $LiMn_2O_4$ powders are typically prepared by a solid-state reaction which consists of extensive mechanical mixing and extended grinding. This treatment is detrimental to the quality of the final product because of the resulting inhomogeneity, irregular morphology, larger particle size with broader particle-size distribution, and poor control of stoichiometry. In order to achieve good efficiency of lithium utilization at high current and high reliability of lithium secondary batteries, a sol–gel method has been introduced. This method produces cathode materials with good homogeneity, uniform morphology and narrow particle-size distribution [3,4]. Recently, we reported [5,6] that spinel $LiMn_2O_4$ powders with pure phase composition and excellent rechargeability can be synthesized by the sol–gel method using Poly(acrylic acid) (PAA) and glycolic acid as a chelating agent. In this work, $LiMn_2O_4$ and $LiMn_{1.95}Ni_{0.05}O_4$ powders with uniform submicron-sized particles are synthesized by the sol–gel method with glycine as a chelating agent at low temperatures and in a short processing time.

Lithium/polymer batteries now being studied extensively as power sources for electric vehicles and portable electronic equipment. The use of a polymer electrolyte makes these batteries safe, flexible, light and thin. Despite a considerable number of reports on the electrical performance of lithium/polymer batteries, few studies have been conducted on the characteristics of the interface between the polymer electrolyte and the electrodes [7–10]. Good interfacial properties between the solid polymer electrolyte and the electrodes are essential to guarantee acceptable performance and cycle-life.

In this paper, the capacity and cycling performance of a Li/polymer electrolyte/$LiMn_{2-x}Ni_xO_4$ cell are evaluated, and the cause of capacity fading during cycling is

* Corresponding author. Tel.: +82-42-865-4074; Fax: +82-42-865-4061; E-mail: yksun@saitgw.sait.samsung.co.kr

0378-7753/99/$ - see front matter
PII: S0378-7753(99)00160-3

investigated in terms of interfacial characteristics by means of a.c. impedance measurements at various temperatures.

2. Experimental

$LiMn_2O_4$ or $LiMn_{1.95}Ni_{0.05}O_4$ powders were prepared according to the procedure shown in Fig. 1. A stoichiometric amount of Li, Mn, and Ni acetate (Acros, high purity) salts with a cationic ratio of Li:Mn = 1:2 or Li:Mn:Ni = 1:1.95:0.05 were dissolved in distilled water and mixed well with an aqueous solution of glycine (Aldrich, high purity). The glycine was used as a chelating agent to produce a gel, and the molar ratio of glycine to total metal ions was fixed at unity. Ammonium hydroxide was added slowly to this solution with constant stirring until a pH of 5 ~ 7.5 was achieved. The resultant solution was evaporated at 70 to 80°C for 5 h until a transparent sol was obtained. To remove water, the sol was heated at 70 to 80°C while being mechanically stirred. As the evaporation of water proceeded, the sol turned into a viscous transparent gel. The resulting gel precursors were decomposed at 300 to 800°C for 10 h in air to obtain phase-pure polycrystalline $LiMn_2O_4$ or $LiMn_{1.95}Ni_{0.05}O_4$ powders.

Powder X-ray diffraction (Rint-2000, Rigaku) using CuK_α radiation was used to identify the crystalline phases of the materials calcined at various temperatures. Rietveld refinement was then performed on the X-ray diffraction data to obtain lattice constants. The change in the particle morphology was observed using a field-emission scanning electron microscope (TOPCON, ABT-150F). The specific surface area of the material was determined by the Brunauer–Emmett–Teller (BET) method (Autosorb-1, Quantachrome) with nitrogen adsorption.

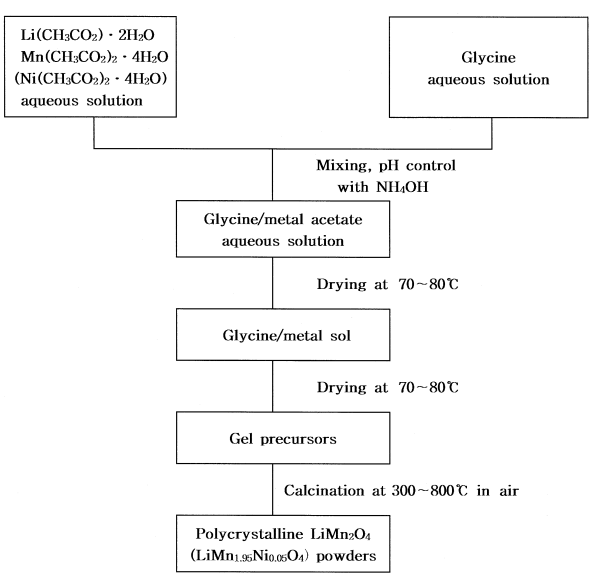

Fig. 1. Flowsheet of procedure used to prepare polycrystalline $LiMn_2O_4$ powders by a glycine-assisted sol–gel method.

The electrochemical properties of $LiMn_{2-x}Ni_xO_4$ powder were determined in Li/polymer electrolyte/$LiMn_{2-x}Ni_xO_4$ cells. The polymer electrolyte was made from polyacrylonitrile (PAN), plasticized by a solution of $LiClO_4$ in a 1:1 mixture of ethylene carbonate (EC) and propylene carbonate (PC). A typical polymer electrolyte composition was 12 wt.% PAN–40 wt.% EC–40 wt.% PC–8 wt.% $LiClO_4$ [11]. The ionic conductivity of the free-standing polymer electrolyte was $2 \times 10^{-3}\ \Omega^{-1}\ cm^{-1}$ at room temperature. The composite cathode was made from $LiMn_2O_4$ spinel powder (89.5 wt.%), acetylene black (5.5 wt.%), and PAN binder(5 wt.%). The $LiMn_2O_4$ spinel powder and acetylene black were added to PAN solution in dimethyl sulfoxide (DMSO) as a solvent. The slurry was spread on to an aluminium foil current-collector, and dried at 110°C in air. The dried composite cathode was then compressed with a roll presser and dried further under vacuum for >10 h at 110°C. A three-electrode cell was used for the electrochemical measurements. The reference and counter electrodes each consisted of lithium foil of 50 μm thickness (Cyprus Foote Mineral) pressed on to a copper current-collector. A rechargeable lithium/polymer cell was assembled by sandwiching the polymer electrolyte between the lithium anode and the composite cathode, and then the reference electrode was placed on the composite cathode side. The cell was enclosed in a metallized plastic bag and vacuum sealed. All cells were assembled in a dry-box filled with argon. The cells were typically cycled between cut-off voltages of 3.4 and 4.3 V at a constant current density of 0.15 mA cm^{-2}, unless otherwise noted. The cells were activated by conducting a cycle at various temperatures (-10, 25, 40, and 50°C). The a.c. impedance measurements were performed using a Zahner Elektrik IM6 impedance analyzer over the frequency range 1 mHz to 100 kHz with an a.c. amplitude of 5 mV_{rms}. Each sample was allowed to equilibrate for 30 min at each cycle before measurement at the fully charged state.

3. Results and discussion

The transparent gel could be formed for all of the ratios of glycine to total metal ions examined in this study. The transparency and uniform color of the gel precursors indicated the formation of a homogeneous phase. It is thought that the carboxylic and amino groups on the glycine can form chemical bonds with the metal ions and that these mixtures develop extremely viscous polymeric resins as become gels [12,13].

Fig. 2 presents X-ray diffraction (XRD) patterns of $LiMn_2O_4$ powders calcined at various temperatures and $LiMn_{1.95}Ni_{0.05}O_4$ powders, calcined at 800°C for 10 h in air. The materials calcined at 200°C are amorphous with no diffraction peaks. After increasing the temperature to 220°C, however, a poorly crystalline $LiMn_2O_4$ phase is

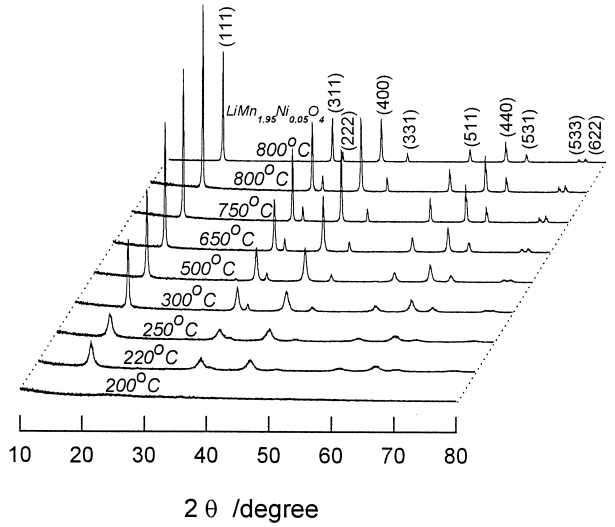

Fig. 2. X-ray diffraction patterns for $LiMn_2O_4$ powders calcined at various temperatures and $LiMn_{1.95}Ni_{0.05}O_4$ powder calcined at 800°C for 10 h in air.

formed. Impurity peaks, corresponding to Li_2CO_3, MnO_2, and Mn_2O_3, are not observed. Such peaks are often found with other low-temperature techniques. On increasing the calcination temperature, diffraction peaks become much sharper with a shift towards the low-angle side in the XRD pattern. This indicates a gradual growth in the average particle size and an increase in the crystallinity of the $LiMn_2O_4$ powders. The gel precursors are crystallized into phase-pure $LiMn_2O_4$ spinel powders without development of a minor phase throughout the calcination temperature range. The XRD patterns of the $LiMn_{1.95}Ni_{0.05}O_4$ powders can be indexed to the same space group (Fd3m) as pure $LiMn_2O_4$ spinel. The use of glycine greatly suppresses the formation of precipitates, from which heterogeneity would arise, because the cross-linked gel may provide more-homogeneous mixing of the cations and little tendency for segregation during calcination. Therefore, the fine-mixture state of the calcined materials in a homogeneous composition makes it possible to form a single-phase spinel $LiMn_2O_4$ under mild conditions. Similar results have been reported [5,6] for $LiMn_2O_4$ and $Li_{1.03}Mn_2O_4$ powders synthesized by the sol–gel method using PAA and glycolic acid as a chelating agent, respectively.

Fig. 3 shows the effect of the calcination temperature on the lattice constant (a), obtained from Rietveld refinement of the XRD patterns and the specific surface area of the same material (as shown in Fig. 2). The lattice constant increases almost linearly up to 8.2260 Å when the calcination temperature increases from 220 to 800°C. The value of the average oxidation state of manganese in the spinel phase is related closely to the lattice constant of the cubic unit cell [14–16]. Lower calcination temperatures result in the formation of a more-oxidized Mn cation because Mn ions are stable as Mn^{4+} at lower temperatures [17]. For example, MnO_2 (with all Mn^{4+}) transforms progressively to Mn_2O_3 (with all Mn^{3+}) for the binary Mn oxide system as temperature increases. The atomic radius of Mn^{3+} (0.72 Å) is larger than that of Mn^{4+} (0.67 Å), and thus the lattice constant of the cubic unit cell of the spinel $LiMn_2O_4$ powders calcined at higher temperatures is larger than that of those calcined at lower temperatures. The probability of cation mixing between Li^+ and Mn^{4+} ions is very high because of the displacement of Li^+ from the 8a site to the 16d site or Mn^{4+} from the 16d site to the 8a site in the spinel $LiMn_2O_4$ calcined at lower temperature, due to the similarity of the ionic radii of Li^+ (0.60 Å) and Mn^{4+} (0.67 Å). It has been reported [14] that the $LiMn_2O_4$ host calcined at 300°C contains either some amount of vacancies on Mn sites (16d) or displacement of Li ions from 8a sites to 16d sites. The lattice constant of $LiMn_{1.95}Ni_{0.05}O_4$ powder calcined at 800°C is 8.2236 Å which is in agreement with the literature value of 8.228 Å for a similar composition [4]. The substitution of Mn with divalent Ni increases the average oxidation state of Mn above 3.5 to maintain electrical neutrality. As a result, the lattice constant of the $LiMn_{1.95}Ni_{0.05}O_4$ host structure is lower than that of the pure spinel. The specific surface area of the powders decreases linearly with increasing calcination temperature, due to the growth of $LiMn_2O_4$ crystallites. Materials calcined at 300 and 800°C have a specific surface area of 25.3 and 2.5 $m^2\ g^{-1}$, respectively.

Scanning electron micrographs (SEM) of $LiMn_2O_4$ powders calcined at various temperatures for 10 h in air are shown in Fig. 4. The presence of loosely agglomerated spherical particles with an average grain size of 50 nm is detected in powders calcined at 300°C (Fig. 4a). As the calcination temperature is increased, the growth kinetics are favored and thus agglomerated spherical particles transform into larger particulates. When the gel precursors are heated at 650 and 750°C, the particle sizes of the particulates increase to 100 and 200 nm, respectively

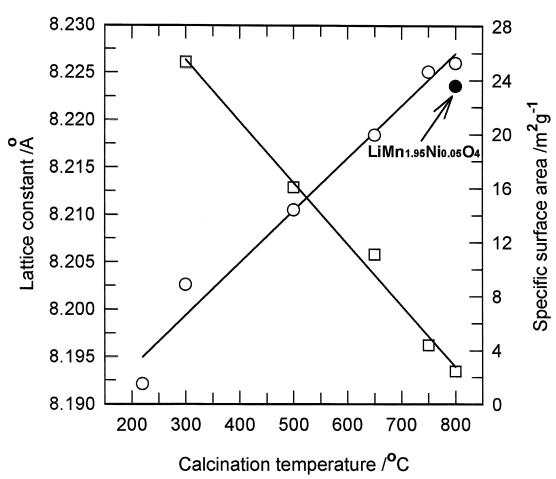

Fig. 3. Effect of calcination temperature on lattice constant and specific surface area of $LiMn_2O_4$ powders. (●) Lattice constant of $LiMn_{1.95}Ni_{0.05}O_4$ powder calcined at 800°C.

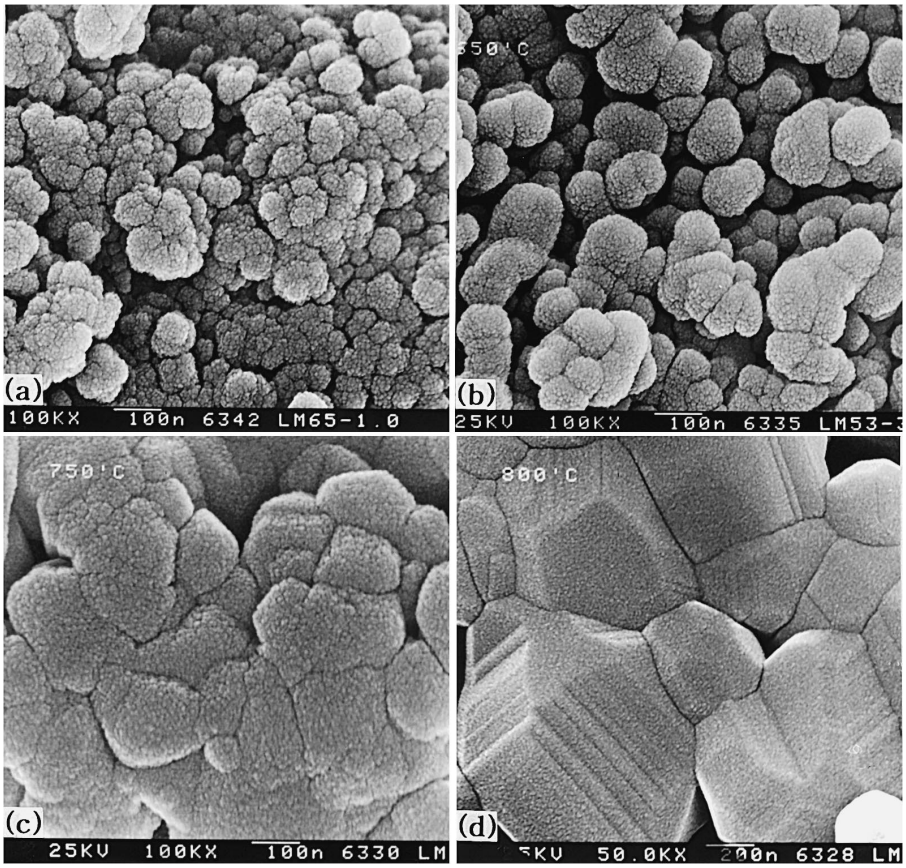

Fig. 4. Scanning electron micrographs of the $LiMn_2O_4$ powders calcined at (a) 300, (b) 650, (c) 750 and (d) 800°C.

(Fig. 4b and c). For materials calcined at 800°C, the particle size of the particulates increases abruptly to about 1 μm (Fig. 4d).

From the above results, we conclude that $LiMn_2O_4$ powders with a wide variety of the physicochemical properties, such as particle size, crystallity, specific surface area, and microcrystallite morphologies can be produced in a controlled manner by simply varying the pyrolysis processing.

The charge–discharge curves (variation of specific discharge capacity) with cycling of a Li/polymer electrolyte/$LiMn_2O_4$ and a $LiMn_{1.95}Ni_{0.05}O_4$ cell at 25°C are shown in Fig. 5a and b, respectively. The $LiMn_2O_4$ and $LiMn_{1.95}Ni_{0.05}O_4$ powders were calcined at 800°C. In the case of the Li/polymer electrolyte/$LiMn_2O_4$ cell, two distinct potential plateau appeared in the charge–discharge curve near 4.0 $V_{Li/Li+}$ and 4.16 $V_{Li/Li+}$. The occurrence of the potential plateau near 4.0 $V_{Li/Li+}$ is due to the co-existence of $Li_{0.5}Mn_2O_4$ and $LiMn_2O_4$, and the plateau near 4.16 $V_{Li/Li+}$ is the result of the coexistence of λ-MnO_2 and $Li_{0.5}Mn_2O_4$. For the Ni-doped spinel electrode, the two-staged potential plateau in the charge–discharge curve became less distinct. This behavior suggests that the substitution of Ni ions results in a locally disordered crystallographic structure. Moreover, local distortion may eliminate the small Li–Li repulsion energy difference between the half-filled 8a sites in $Li_{0.5}Mn_2O_4$ and the completely filled sites in $LiMn_2O_4$ and give rise to a relatively random Li occupation.

The initial capacity of the Li/polymer electrolyte/$LiMn_2O_4$ cell is 145 mA h g^{-1} and the discharge capacity decreases slowly with cycling. The theoretical capacity of $LiMn_2O_4$ is 148 mA h g^{-1}, but this value has never been obtained in practice. Often, the material with the highest capacity exhibits the highest degree of capacity fade. For example, we have found [5] that $Li_{1.03}Mn_2O_4$ with a lower initial capacity of 133 mA h g^{-1} [5] displayed significantly better cycle-life in comparison with stoichiometric $LiMn_2O_4$. As shown in Fig. 5b, the initial capacity of a cell with a Ni-doped cathode is lower than that for a cell with stoichiometric $LiMn_2O_4$. This suggests that even for the substituted spinel phase, only the amount of Mn^{3+} contributes to the charge–discharge capacity, because Li intercalation into and deintercalation from the spinel structure must be electrically compensated by the oxidation of Mn^{3+} to Mn^{4+}. Cycle-life is improved, however, at the expense of capacity by this substitution. This can be explained by postulating that doped Ni ions enhance the stability of the octahedral sites in the spinel skeleton structure due to the strength of the Ni–O bonds in the structure. In comparison with $LiMn_2O_4$ (Fig. 5a), the capacity of $LiMn_{1.95}Ni_{0.05}O_4$ (Fig. 5b) decreases more

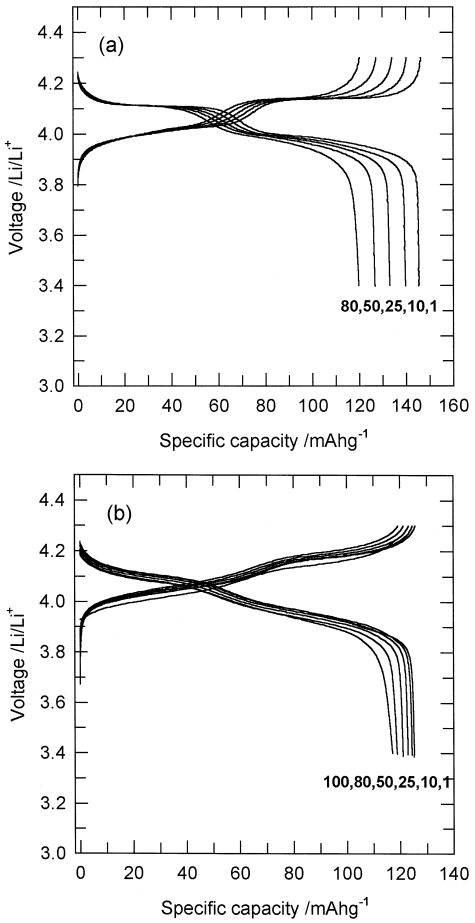

Fig. 5. Charge–discharge curves (variation of specific discharge capacity) with cycle number for Li/polymer electrolyte/(a) $LiMn_2O_4$/and (b) $LiMn_{1.95}Ni_{0.05}O_4$ cells. Cycling carried out galvanostatically at a constant charge and discharge current density of 2 mA cm^{-2} between 3.4 and 4.3 $V_{Li/Li+}$.

slowly during cycling and remains at 120 mA h g^{-1} at the 100th cycle. This value is somewhat lower than 128 mA h g^{-1} for $Li_{1.03}Mn_2O_4$ at the 90th cycle (96% of its initial capacity). As mentioned, this indicates better cyclability of $LiMn_{1.95}Ni_{0.05}O_4$ compared with $LiMn_2O_4$.

In order to explore the performance of the cell Li/polymer electrolyte/$LiMn_{1.95}Ni_{0.05}O_4$ in detail, variations in the specific discharge capacity and the a.c.-impedance spectrum with respect to the number of cycles were measured at various operating temperatures. The $LiMn_{1.95}Ni_{0.05}O_4$ powder was calcined at 800°C. The variation of discharge capacity with cycling at various temperatures is shown in Fig. 6. The discharge capacity at 25°C (Fig. 6a) decreases slowly during cycling, and after 100 cycles about 95% of the initial capacity can be recovered. By contrast, the capacity fading during cycling is faster at cell temperatures of 40°C (Fig. 6c) and 50°C (Fig. 6d); the capacity loss was 50% of the initial value after 80 cycles at 40°C and 20 cycles at 50°C. According to studies by Xia and Yoshio [18] on the performance of Li-ion cells with spinel $LiMn_2O_4$ electrodes, the capacity fading during cycling at 50°C is about 19% of the initial discharge capacity of 130 mA h g^{-1} for the first 50 cycles. The authors suggested that the capacity loss for a cell cycled at 50°C is due mainly to Mn dissolution and is more serious at high temperature than at low temperature. As shown in Fig. 6, there is no capacity fading at −10°C (Fig. 6b) to 80 cycles. From the present results, the discharge capacity loss at 40 and 50°C is much larger than that for a lithium-ion cell with a spinel $LiMn_2O_4$ electrode. Although Mn dissolution in a gel-type polymer electrolyte system is not so severe as that in a liquid electrolyte, its contribution to the capacity loss is not negligible. It can be expected that the reduced capacity at high temperature is attributable to other factors than Mn dissolution. Therefore, a.c.-impedance analysis of the interfacial reaction between the electrolyte and the electrode may provide a better understanding of the cycling performance of the lithium/polymer cell.

Typical Nyquist plots obtained from a Li/polymer electrolyte/$LiMn_{1.95}Ni_{0.05}O_4$ cell in its charged state with respect to number of cycles at 25, 40, and 50°C are shown in Fig. 7a, b and c, respectively. The impedance spectra at 25°C consist of two arcs in the high and intermediate frequency ranges, a line inclined at constant angle to the real axis in the low-frequency range of 10 mHz to 50 mHz, and a capacitive line due to the accumulation of lithium ions at the center of the oxide particle in the frequency range below 10 mHz. The two arcs in the higher frequency range may be due to the reaction at the electrolyte/oxide-electrode interface, and the inclined line in the lower frequency range is attributed to the Warburg impedance which is associated with lithium-ion diffusion through the oxide electrode. The temperature dependence of the impedance spectra was measured to investigate which part of the impedance for the electrode corresponds to the reaction at the electrolyte/oxide-electrode interface. A change in diameter of the first arc with temperature indi-

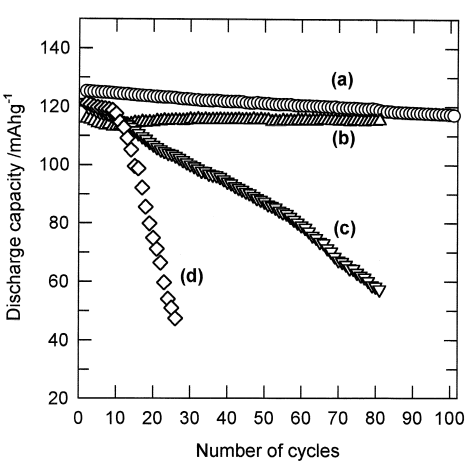

Fig. 6. Variation of specific discharge capacity with cycle number for Li/polymer electrolyte/$LiMn_{1.95}Ni_{0.05}O_4$ cell at various temperatures: (a) 25, (b) −10, (c) 40, (d) 50°C.

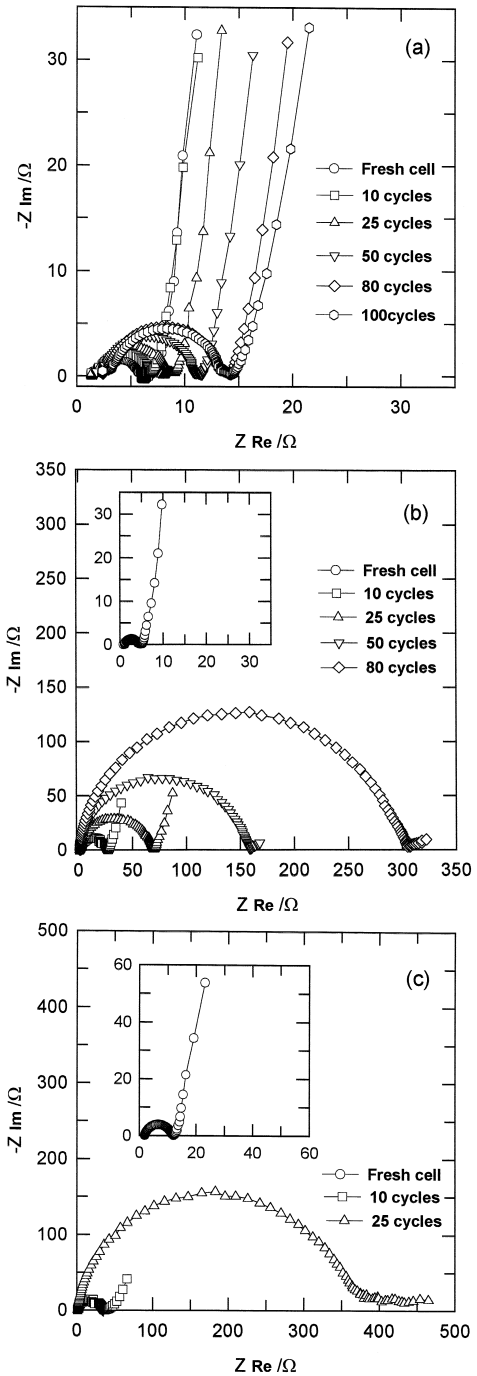

Fig. 7. Typical Nyquist plots obtained from Li/polymer electrolyte/$LiMn_{1.95}Ni_{0.05}O_4$ cell in charged state at (a) 25, (b) 40 and (c) 50°C with respect to cycle number.

cates an activation energy of 10^{-4} eV, which is too small to be indicative of a charge-transfer reaction. It has been reported [19,20] that the magnitude of the high-frequency arc increases with increasing oxide-electrode mass but decreases with increasing amounts of carbon used as a conducting agent. These findings suggest that the high-frequency arc represents particle-to-particle contact resistance and capacitance within the oxide particles, and that the intermediate-frequency arc is related to the reaction at electrolyte/cathode (oxide electrode) interface. As the number of cycles increases, the magnitude of the intermediate-frequency arc remains nearly constant irrespective of cycling, whereas the magnitude of the high-frequency arc increases monotonically with cycling and indicates deterioration of contact with the cathode as a result of volume changes of the cathode during charge–discharge cycling. By contrast, the interface between the electrolyte and the cathode can be regarded as stable during cycling, because of the nearly invariant resistance of the electrolyte/cathode interface up to 100 cycles. Thus, the discharge capacity loss during cycling due to degradation of the electrolyte/cathode interface can be considered as negligible in our cell. At temperatures above 25°C, only one arc appears. Because the electrolyte/cathode interfacial resistance may decrease with increasing temperature, the contact resistance of the composite cathode dominates over the electrolyte/cathode interfacial resistance. It is should be noted that the contact resistance is much larger at 50°C than at 40°C during charge–discharge cycles. From this result, it can be inferred that the enhanced decline in discharge capacity of the Li/polymer electrolyte/Li-$Mn_{1.95}Ni_{0.05}O_4$ cell at high temperature may be related to degradation of the contact within the oxide electrode as well as Mn dissolution.

The value of the apparent chemical diffusivity, $\tilde{D}_{Li^+}$, of Li ions in a porous $LiMn_{1.95}Ni_{0.05}O_4$ electrode at various temperatures with respect to cycle number was calculated using the relation [21]:

$$\tilde{D}_{Li^+} = \frac{\pi f_T r^2}{1.94} \quad (1)$$

where f_T is the frequency at which the impedance spectrum shows a transition from semi-infinite diffusion behavior to finite-length diffusion behavior. The f_T value was determined from Fig. 7. The average radius, r, of the oxide particle was determined from SEM observations.

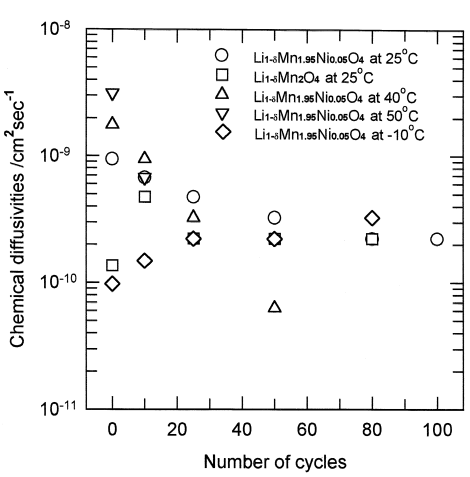

Fig. 8. Chemical diffusion of lithium ions in a porous $LiMn_{1.95}Ni_{0.05}O_4$ electrode as a function of cycle number at various temperatures.

The calculated chemical diffusion of Li ions in $LiMn_{1.95}Ni_{0.05}O_4$ at various temperatures is plotted as a function of cycle number in Fig. 8. The chemical diffusion coefficient values ranged from 10^{-8} to 10^{-11} cm^2 s^{-1} and (except at $-10°C$) decrease during charge–discharge cycling. The increase in diffusion coefficient with cycling at $-10°C$ can be ascribed to improved Li transfer during cycling that results from an initial poor interfacial contact between the electrolyte and the electrode in the fresh state. As shown in Fig. 7, the Li-ion chemical diffusion coefficient is larger at higher temperatures in the initial state, but decreases markedly during cycling at higher temperatures. Because the Li intercalation reaction into the oxide electrode consists of consecutive steps, it can be inferred that a larger contact resistance upon cycling at higher temperatures is responsible for slower chemical diffusion rates upon cycling. From these results, it should be noted that the Li-ion chemical diffusion coefficient decreases markedly upon cycling at higher temperature. The reduced diffusion rate, as well as the increased contact resistance and Mn dissolution, can account for the enhanced decline in discharge capacity of the Li/polymer electrolyte/$LiMn_{1.95}Ni_{0.05}O_4$ cell.

4. Conclusions

Spinel $LiMn_2O_4$ powders with sub-micron, mono-dispersed, and highly homogeneous particles have been synthesized by a sol–gel method using an aqueous solution of metal acetate containing glycine as a chelating agent. Polycrystalline $LiMn_2O_4$ powders are found to be composed of very uniformly sized particulates with an average particle size of 0.05 to 1 μm and a specific surface area of 2.5 to 5.3 m^2 g^{-1}. The initial capacity of a cell with a $LiMn_{1.95}Ni_{0.05}O_4$ cathode is lower than that with stoichiometric $LiMn_2O_4$, but the cycle performance is improved at the expense of capacity by this substitution. This behavior can be explained by postulating that the presence of Ni ions enhances the stability of the octahedral sites in the spinel skeleton structure. From an analysis of a.c.-impedance spectra at various temperatures, it can be inferred that the enhanced decline in discharge capacity for a Li/polymer electrolyte/$LiMn_{1.95}Ni_{0.05}O_4$ cell at high temperature is related to the contact resistance within the oxide electrode as well as to reduced Li-ion diffusion rates and Mn dissolution during cycling.

References

[1] T. Ohuzuka, M. Kitagawa, T. Hirai, J. Electrochem. Soc. 137 (1990) 760.
[2] D. Guyomard, J.M. Tarascon, Solid State Ionics 69 (1994) 222.
[3] T. Tsumura, A. Shimizu, M. Inagaki, J. Mater. Chem. 3 (1993) 995.
[4] W. Liu, G.C. Farrington, F. Chaput, B. Dunn, J. Electrochem. Soc. 143 (1996) 879.
[5] Y.-K. Sun, Solid State Ionics 100 (1997) 115.
[6] Y.-K. Sun, I.-H. Oh, K.W. Kim, Ind. Eng. Chem. Res. 36 (1997) 4839.
[7] B.C.H. Steele, G.E. Lagos, P.C. Spurdens, C. Forsyth, A.D. Foord, Solid State Ionics 9/10 (1983) 391.
[8] R. Koksbang, I.I. Olsen, P.E. Tonder, N. Knudsen, D. Fauteux, J. Electrochem. Soc. 21 (1991) 301.
[9] D. Fauteux, J. Electrochem. Soc. 135 (1988) 2231.
[10] A. Selvaggi, F. Croce, B. Scrosati, J. Power Sources 32 (1990) 389.
[11] Z. Jiang, K.M. Abraham, J. Electrochem. Soc. 143 (1996) 1591.
[12] P.A. Lessing, Ceram. Bull. 68 (1989) 1002.
[13] M.S.G. Baythoun, F.R. Sale, J. Mater. Sci. 17 (1982) 2757.
[14] T. Tsumura, M. Inagaki, Solid State Ionics 104 (1997) 36.
[15] C. Tsang, A. Manthiram, Solid State Ionics 89 (1996) 305.
[16] D.H. Jang, Y.J. Shin, S.M. Oh, J. Electrochem. Soc. 143 (1996) 2204.
[17] C. Masquelier, M. Tabuchi, K. Ado, R. Kanno, Y. Kobayashi, Y. Maki, O. Nakamura, B. Goodenough, J. Solid State Chem. 123 (1996) 255.
[18] Y. Xia, M. Yoshio, J. Electrochem. Soc. 143 (1996) 100.
[19] Y.-M. Choi, S.-I. Pyun, J.-S. Bae, S.-I. Moon, J. Power Sources 56 (1995) 15.
[20] S.-I. Pyun, J.-S. Bae, Electrochim. Acta 41 (6) (1996) 919.
[21] R. Cabanel, T. Barral, J.-P. Diard, B. Le Gorrec, C. Montella, J. Appl. Electrochem. 23 (1993) 93.